Three-Phase SRF PLL Model for System Frequency Response Studies in Low-Inertia Systems

Matej Krpan*, Igor Erceg†, Igor Kuzle* and Hrvoje Pandžić*
*Department of Energy and Power Systems
†Department of Electric Machines, Drives and Automation
University of Zagreb Faculty of Electrical Engineering and Computing
Zagreb, Croatia
Email: matej.krpan@fer.hr, igor.erceg@fer.hr, igor.kuzle@fer.hr, hrvoje.pandzic@fer.hr

***Abstract*—This paper derives a small-signal model of a three-phase synchronous reference frame phase-locked loop for use in system frequency response studies assuming a system of balanced three-phase voltages. The small-signal model is described by a second-order transfer function which relates the actual to the estimated grid frequency. The small-signal model behaves identically to the large-signal model for small disturbances. Simulation results demonstrate that phase-locked loop dynamics can be neglected in the high-inertia scenarios, while in the low-inertia scenarios they have a significant impact on the grid frequency and should be included in models.**

***Index Terms*—grid-following converters, low-inertia power system, phase-locked loop, PLL, small-signal model, synchronous reference frame, system frequency response**

I. Introduction and motivation

There is a clear trend of massive penetration of power electronic devices in the power systems worldwide, which magnifies the previously negligible dynamic behaviour and dynamic interactions [1], [2]. In turn, this introduces new challenges to the power system operation [3]. Integration of converter-interfaced devices results in reduced synchronous inertia which influences the grid frequency dynamics. Moreover, the timescale of power electronics control is faster than the electromechanical dynamics and closer to the electromagnetic phenomena domain [4]—thus, in a system dominated by power electronic devices the dominant time constants are smaller. Majority of converter-interfaced devices today (e.g. wind, solar PV, battery energy storage) are of the grid-following type, meaning that they require a stiff grid as a reference of voltage and frequency. Synchronisation of grid-following converters to the grid voltage is usually achieved via phase-locked loops (PLLs) [5], [6] that introduce a certain time lag to the overall control systems. Naturally, many grid-following converters in a weak grid cannot operate in a stable manner [7], therefore grid-forming control schemes that do not require a PLL for synchronisation are currently a topic of interest in bulk power systems research [8].

Bulk power systems of the future will consist of a mix of grid-following and grid-forming converter-interfaced devices. System operators increasingly require converter-interfaced generators to participate in ancillary services such as frequency control through droop control and/or emulation of synchronous inertia (called virtual or synthetic inertia) [6], [9], [10]. If grid-following units support system frequency, the modulation of output power is based on the grid frequency signal estimated by a PLL. Thus, PLL dynamics may have an influence on the overall frequency control performance [11], [12]. Furthermore, recent research indicates that PLLs should be considered in studies concerning grid frequency dynamics [13], [14].

A commonly used tool for studying grid frequency dynamics are uniform low-order system frequency response (SFR) models [9], [15], [16]. They model the grid as a single machine with equivalent inertia and damping, and the relevant active power control mechanisms (turbine-governors, under-frequency load shedding, synthetic inertia, etc.). Only the slowest time constants are considered, as those will mostly define the frequency dynamics [15]. Grid topology (branches and buses) is not considered in SFR models, therefore there are no voltage dynamics. These models relatively accurately simulate an average behaviour of the grid frequency after a disturbance. In the literature so far, only perfect tracking of the grid frequency for converter-interfaced devices has been assumed, i.e. no PLL dynamics has been considered, [9], [16]–[23]. However, PLL can have a significant influence on the plant response.

Small-signal models of PLLs have been derived and used for various purposes, mostly for analysis and shaping of the input-admittance of voltage source converters [24]–[27]. In these papers, the small-signal modelling was used to derive grid-voltage-to-reference-current [26] and phase-angle-to-grid-voltage PLL transfer functions [24], [25], [27]. Additionally, the impact of grid frequency on phase angle change has been derived in [28]. However, there is no voltage dynamics in SFR models and the phase angle is not relevant for the aggregated machine in SFR models. The transfer function of interest is the one that relates the *true* grid frequency to the grid frequency estimated by a PLL, which has been presented in [29], but detailed derivation procedure was not provided and the transfer function contains the voltage amplitude. Additionally, small-signal PLL impact on grid frequency dynamics was also not analysed in [29]. Therefore, the main contributions of

This work was funded by the European Union through the European Regional Development Fund Operational Programme Competitiveness and Cohesion 2014-2020 of the Republic of Croatia under project KK.01.1.1.04.0034 "Connected Stationary Battery Energy Storage".

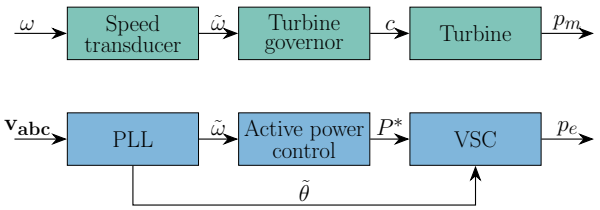

Fig. 1: Analogy between synchronous generators and grid-following VSCs

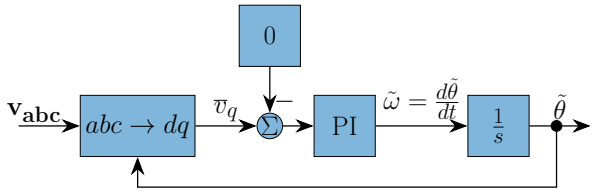

Fig. 2: Three-phase synchronous reference frame PLL

this paper are: (i) detailed derivation procedure of a three-phase synchronous reference frame (SRF/dq) PLL frequency-to-frequency transfer function which is the most interesting for SFR studies; (ii) analysis of the PLL impact on grid frequency using the developed model.

Rest of the paper is organised as follows: in Section II, the methodology and assumptions are described. In Section III the PLL transfer function is derived. In Section IV the small-signal model is validated against a nonlinear model and the impact of PLL on grid frequency in various scenarios is investigated. Finally, Section V concludes the paper.

II. Methodology and Assumptions

An analogy can be drawn between the conventional synchronous generators and the grid-following VSCs, as illustrated in Fig. 1. Voltage control / reactive power control is omitted from this illustration. SG machine speed ω is estimated by a speed transducer. Then, the estimated speed $\tilde{\omega}$ is passed on to a turbine governor which modifies the gate or valve opening c (droop control). The turbine translates the gate/valve opening into mechanical power output p_m at the turbine shaft.

In VSCs, on the other hand, a PLL estimates the grid frequency $\tilde{\omega}$ from the measured voltage $\mathbf{v_{abc}}$ at the point of common coupling. If a VSC operates in the grid-supporting mode, then $\tilde{\omega}$ can be used to modify the active power command P^* (e.g. droop control or virtual inertia). However, the main purpose of a PLL is to extract the phase angle of the grid voltage $\tilde{\theta}$ in order to synchronise with the grid. The VSC block in Fig. 1 contains the inner voltage and current control loops, as well as the PWM modulation for generating gate signals for the inverter. Output of the VSC is the electrical power p_e.

Generally, most generic dynamic models of turbines include the effect of the speed transducer and the governing system [30]. However, (modern) governing systems are much faster than turbine dynamics so their effect is often neglected in SFR models. On the other hand, the time scale of a PLL is also faster than the VSC active power control [4], so it can be inferred that it could also be neglected in SFR studies. However, depending on how PLL gains are tuned, the time lag it induces can have an effect on estimated frequency and, consequently, the performance of active power control [12]–[14], [31]—especially in low-inertia systems.

Regardless, since a PLL estimates the frequency from the measured instantaneous grid voltage, it is mostly susceptible to electromagnetic disturbances such as voltage unbalances, spikes and dips [31], [32]. This paper aims to derive a transfer function of a three-phase SRF PLL which relates the actual grid frequency to the estimated grid frequency suitable for implementation in SFR models which inherently do not capture the voltage dynamics. Such transfer function essentially captures the time lag a PLL introduces into the closed-loop control. The derivation will be based on three assumptions: i) Three-phase voltages are balanced; ii) Voltage amplitudes are constant and close to the nominal value; iii) Only the simplest representation of a SRF PLL is used.

The first two assumptions are valid since SFR models do not consider voltage dynamics—they only model effects of global generation/load imbalance on system's average frequency through the swing equation (generator inertia and load self-regulation) and control reactions (droop control, synthetic inertia, underfrequency load shedding, etc.). The last assumption is to simplify the analysis by using a textbook example of a SRF PLL system. It means that additional filters or more complex PLL structures used to improve rejection of grid voltage harmonics, unbalances and other disturbances are ignored (also, these phenomena are inherently not captured by SFR models).

The three-phase SRF PLL structure used to derive the small-signal model is shown in Fig. 2. The input is a three-phase voltage measurement at the grid connection point $\mathbf{v_{abc}}$ (1), where $\theta = \theta(t)$ is the grid voltage phase angle. PLL estimates the phase angle $\tilde{\theta} = \tilde{\theta}(t)$ such that that the $abc \rightarrow dq$ transformation zeroes out the q-component of voltage (v_q). Normalised (per-unit) component $\overline{v}_q$ is passed through a proportional-integral (PI) controller to obtain the estimate of the grid angular frequency $\tilde{\omega}$ which is then integrated by means of a voltage-controlled oscillator to obtain $\tilde{\theta}$. In steady-state, $\omega = \tilde{\omega}$, $\theta = \tilde{\theta}$, and $v_q = 0$.

$$\mathbf{v_{abc}}^\top = \begin{bmatrix} v_a(\theta(t)) & v_b(\theta(t)) & v_c(\theta(t)) \end{bmatrix} \tag{1}$$

III. Small-signal model of SRF PLL

Referring to the assumptions set in Section II, we consider a three-phase system of AC voltages:

$$v_a = V_a \sin\left(\theta(t)\right) \tag{2a}$$

$$v_b = V_b \sin\left(\theta(t) - \frac{2\pi}{3}\right) \tag{2b}$$

$$v_c = V_c \sin\left(\theta(t) - \frac{4\pi}{3}\right) \tag{2c}$$

where V_a, V_b and V_c are the peak values of phase-to-ground voltages of each phase. $\theta(t)$ is the grid voltage phase angle described by (3). θ_0 is the initial phase angle and $\omega = \omega(t)$ is the grid angular frequency.

$$\theta(t) = \int \omega(\tau)d\tau + \theta_0 \tag{3a}$$

$$\frac{d\theta}{dt} = \omega \tag{3b}$$

Transformation from abc to dq coordinates (neglecting the 0-component for balanced systems) is achieved through the tensor $\mathbf{T_{dq}}$ [5]:

$$\begin{bmatrix} v_d \\ v_q \end{bmatrix} = \frac{2}{3}\mathbf{T_{dq}} \begin{bmatrix} v_a \\ v_b \\ v_c \end{bmatrix} \tag{4}$$

where $\mathbf{T_{dq}} = \mathbf{T_{dq}}(\tilde{\theta}(t))$ is defined as:

$$\mathbf{T_{dq}} = \begin{bmatrix} \sin\left(\tilde{\theta}(t)\right) & \sin\left(\tilde{\theta}(t) - \frac{2\pi}{3}\right) & \sin\left(\tilde{\theta}(t) - \frac{4\pi}{3}\right) \\ \cos\left(\tilde{\theta}(t)\right) & \cos\left(\tilde{\theta}(t) - \frac{2\pi}{3}\right) & \cos\left(\tilde{\theta}(t) - \frac{4\pi}{3}\right) \end{bmatrix} \tag{5}$$

Obviously, the grid voltage angle extracted by the PLL is equal to:

$$\tilde{\theta}(t) = \int \tilde{\omega}(\tau)d\tau + \tilde{\theta}_0 \tag{6a}$$

$$\frac{d\tilde{\theta}}{dt} = \tilde{\omega} \tag{6b}$$

After combining (2), (4) and (5), component v_q is equal to:

$$v_q(t) = \begin{bmatrix} \cos\left(\tilde{\theta}(t)\right) \\ \cos\left(\tilde{\theta}(t) - \frac{2\pi}{3}\right) \\ \cos\left(\tilde{\theta}(t) - \frac{4\pi}{3}\right) \end{bmatrix}^\top \begin{bmatrix} V_a \sin(\theta(t)) \\ V_b \sin\left(\theta(t) - \frac{2\pi}{3}\right) \\ V_c \sin\left(\theta(t) - \frac{4\pi}{3}\right) \end{bmatrix} \tag{7}$$

Assuming a balanced three-phase system with constant voltage amplitudes ($V_a = V_b = V_c = V$), expression (7) reduces to:

$$v_q(t) = V \sin\left(\theta(t) - \tilde{\theta}(t)\right) \tag{8}$$

Equation (8) can be normalised to the voltage amplitude V to obtain the per-unit value of q-component $\overline{v}_q$ from Fig. 2:

$$v_q(t) \mapsto \overline{v}_q(t) = \sin\left(\theta(t) - \tilde{\theta}(t)\right) \tag{9}$$

The goal now is to get rid of the voltage variable $\overline{v}_q$ (since there is no voltage in SFR models) and linearise the system to derive the transfer function from $\Delta\omega$ to $\Delta\tilde{\omega}$. To achieve this, the nonlinear dynamical system of SRF PLL is described by the following system of differential equations:

$$\frac{d\theta}{dt} = \omega \tag{10a}$$

$$\frac{d\xi}{dt} = \sin\left(\theta - \tilde{\theta}\right) = \overline{v}_q \tag{10b}$$

$$\frac{d\tilde{\theta}}{dt} = K_p \sin\left(\theta - \tilde{\theta}\right) + K_i\xi = \tilde{\omega} \tag{10c}$$

where K_p and K_i are the proportional and integral gain of the PI controller (Fig. 2) described by the transfer function $H(s) = K_p + K_i s^{-1}$.

$\Delta\overline{v}_q$ is a multivariate function linearised as follows:

$$\Delta\overline{v}_q \approx \left.\frac{\partial\overline{v}_q}{\partial\theta}\right|_{(\theta_0,\tilde{\theta}_0)} \Delta\theta + \left.\frac{\partial\overline{v}_q}{\partial\tilde{\theta}}\right|_{(\theta_0,\tilde{\theta}_0)} \Delta\tilde{\theta} \tag{11a}$$

$$= \cos\left(\theta_0 - \tilde{\theta}_0\right)\Delta\theta - \cos\left(\theta_0 - \tilde{\theta}_0\right)\Delta\tilde{\theta} \tag{11b}$$

$$= \Delta\theta - \Delta\tilde{\theta} \tag{11c}$$

since $\theta_0 = \tilde{\theta}_0$ in the steady-state. Linearising eq. (10a) results in (12), and $\Delta\omega$ is set as the input (perturbation) variable $\Delta u(t)$:

$$\frac{d\Delta\theta}{dt} = \Delta\omega = \Delta u(t) \tag{12}$$

Linearising (10c) results in (13), and $\Delta\tilde{\omega}$ is set as the output variable $\Delta y(t)$:

$$\frac{d\Delta\tilde{\theta}}{dt} = \Delta\tilde{\omega} = \Delta y(t) \tag{13}$$

Finally, the state-space model can be written combining (11)–(13):

$$\Delta\dot{\mathbf{x}} = \mathbf{A}\Delta\mathbf{x} + \mathbf{B}\Delta\mathbf{u} \tag{14a}$$

$$\Delta\mathbf{y} = \mathbf{C}\Delta\mathbf{x} + \mathbf{D}\Delta\mathbf{u} \tag{14b}$$

where $\Delta\mathbf{x}$, $\Delta\mathbf{u}$, $\Delta\mathbf{y}$, $\mathbf{A}$, $\mathbf{B}$, $\mathbf{C}$ and $\mathbf{D}$ are equal to:

$$\Delta\mathbf{x} = \begin{bmatrix} \Delta\theta & \Delta\xi & \Delta\tilde{\theta} \end{bmatrix}^\top \tag{15a}$$

$$\Delta\mathbf{u} = \Delta u = \Delta\omega \tag{15b}$$

$$\Delta\mathbf{y} = \Delta y = \Delta\tilde{\omega} \tag{15c}$$

$$\mathbf{A} = \begin{bmatrix} 0 & 0 & 0 \\ 1 & 0 & -1 \\ K_p & K_i & -K_p \end{bmatrix} \tag{15d}$$

$$\mathbf{B} = \begin{bmatrix} 1 & 0 & 0 \end{bmatrix}^\top \tag{15e}$$

$$\mathbf{C} = \begin{bmatrix} K_p & K_i & -K_p \end{bmatrix} \tag{15f}$$

$$\mathbf{D} = 0 \tag{15g}$$

The SRF PLL transfer function is now equal to (16), which corresponds to the form from [29] neglecting the voltage amplitude:

$$G_{pll}(s) = \frac{\Delta y(s)}{\Delta u(s)} = \frac{\Delta\tilde{\omega}}{\Delta\omega} = \frac{\Delta\tilde{f}}{\Delta f} \tag{16}$$

$$= \mathbf{C}\left[s\mathbf{I} - \mathbf{A}\right]^{-1}\mathbf{B} + \mathbf{D}$$

$$= \frac{K_p s + K_i}{s^2 + K_p s + K_i}$$

$G_{pll}(s)$ exhibits a generic second-order system dynamics (17), where natural frequency ω_n and damping factor ζ are defined as (18) and (19), respectively. T_i is the integrator reset time.

$$\mathcal{G}(s) = \frac{2\zeta\omega_n s + \omega_n^2}{s^2 + 2\zeta\omega_n s + \omega_n^2} \tag{17}$$

$$\omega_n = \sqrt{K_i} = \sqrt{\frac{K_p}{T_i}} \tag{18}$$

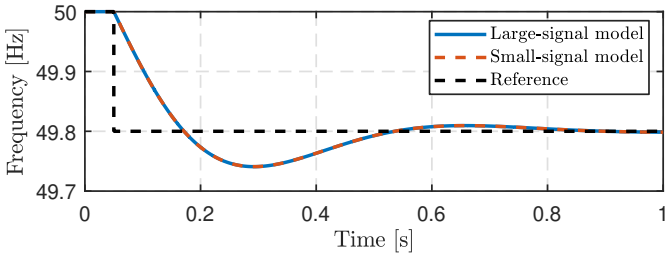

Fig. 3: Validation of the small-signal SRF PLL model

$$\zeta = \frac{K_p}{2\omega_n} = \sqrt{\frac{K_p T_i}{4}} \tag{19}$$

Depending on how the gains are tuned, the PLL will have more or less damped oscillatory behaviour. The input derivative ($2\zeta\omega_n s$ member in the numerator) mostly influences the high-frequency behaviour by introducing the $+90$ degree phase-shift and reducing the magnitude fall-off by 20 dB/decade.

IV. Validation of Small-Signal Model and Grid Impact Analysis

A. Validation via the step response test

The small-signal model of a three-phase SRF PLL (16) is compared against the large-signal model from Fig. 2 for a step change in frequency of $\Delta f = -0.2$ Hz. The PLL parameters are $K_p = 10$ and $K_i = 100$. K_p and K_i are tuned based on trial-and-error until a satisfying performance was achieved without being too aggressive, similar to [28]. Results show (Fig. 3) that the small-signal model perfectly describes the large-signal model thus confirming the correctness of the small-signal model derivation procedure from Section III.

B. Impact of PLL on grid frequency

Consider a simple power system model shown in Fig. 4 consisting of a converter unit described by droop gain K_c and time constant T_c, and a conventional synchronous turbine-generator described by droop gain K_1 and time constants T_1 and T_2. Active power disturbance is denoted with δp_d. Simulations are conducted in MATLAB-Simulink.

We consider two scenarios: high-inertia and low-inertia. In the high-inertia scenario, the parameters are set as follows: $H = 5$ s, $D = 1$ p.u., $T_1 = 2.4$ s, $T_2 = 8$ s — simulating a system of large synchronous generators with slow steam turbine dynamics [30]. In the low-inertia scenario, $H = 1$ s, $D = 1$ p.u., $T_1 = 0$ s, $T_2 = 0.3$ s — simulating a system with a low share of synchronous generators with faster turbine dynamics, e.g. gas turbines [33]. In both scenarios, $K_1 = K_c = 20$ p.u. (equivalent to 5% droop), $T_c = 0.01$ s, and PLL parameters are $K_p = 10$, $K_i = 100$. The disturbance value is set to $\delta p_d = -0.1$ p.u. at $t = 0.5$ s.

Results for both scenarios are shown in Fig. 5. It can be seen that for the high-inertia scenario, the impact of PLL is negligible since the grid frequency change is much slower (Fig. 5, top). Therefore, PLL ($\Delta\tilde{f}$) can easily track the strong

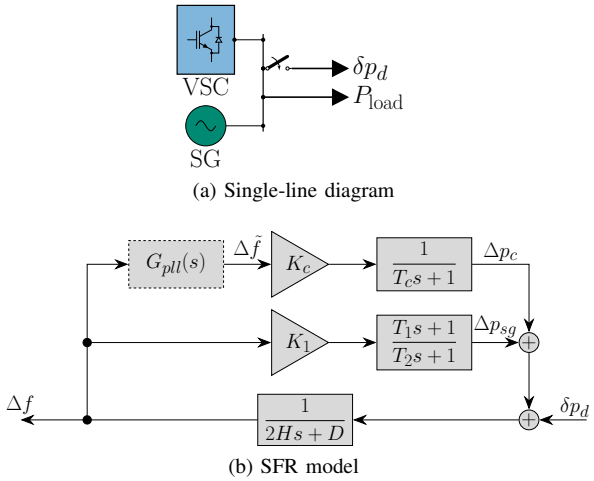

(a) Single-line diagram

(b) SFR model

Fig. 4: Simple test system consisting of a grid-following converter, synchronous generator and load disturbance

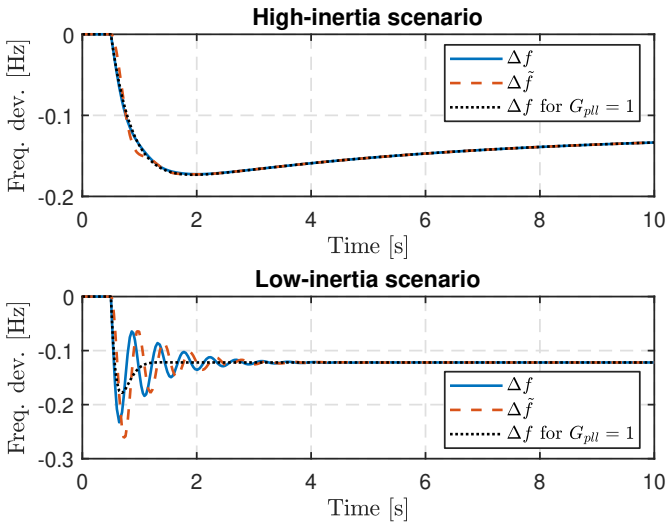

Fig. 5: Impact of PLL dynamics on grid frequency

grid frequency (Δf). In such case, no significant error will be induced if $G_{pll}(s)$ is neglected (dotted line in Fig. 5, top).

On the other hand, in the low-inertia scenario (Fig. 5, bottom), the PLL impact is significantly more pronounced — firstly, PLL has a much tougher time tracking the actual grid frequency ($\Delta\tilde{f}$ compared to Δf) judging by the maximum deviation and the phase-shift. Secondly, if the PLL is neglected (dotted line in Fig. 5, bottom) the induced error is much greater. The maximum frequency deviation is $\approx$ 50 mHz smaller, the settling time is $\approx$ 1 s faster and there are no oscillations in the frequency giving a much more optimistic prediction. Thus, in the low-inertia scenario, the PLL dynamics play a more significant role and should be included in the SFR studies. Improved tracking can be achieved by increasing K_p and K_i. However, unnecessarily high PLL bandwidth is generally avoided due to a negative impact on the converter passivity [34].

V. Conclusion

In this paper, a small-signal model of a three-phase PLL in the synchronous reference frame for inclusion in low-order system frequency response models was derived. The small-signal model is developed assuming a balanced three-phase system with constant voltage amplitude. In this case it exhibits a second-order system dynamic behaviour whose parameters only depend on the gains of the proportional-integral controller. The derived small-signal model captures the time lag of estimating the instantaneous grid frequency deviation used for grid-supporting ancillary services. Results indicate that in the case of a high-inertia system with slower control dynamics, PLL can be neglected in system frequency response studies since the grid frequency changes at a slow rate. In case of a low-inertia system with faster control dynamics, PLL increases oscillations, frequency nadir (by 50 mHz), and settling time (by 1 s). Therefore, it should be included in the system frequency response models of low-inertia systems.

Future work will involve small-signal modelling of other types of phase-locked loops and synchronisation techniques as well as a more detailed PLL impact analysis on higher-fidelity power system models.

References

[1] F. Milano, F. Dorfler, G. Hug, D. J. Hill, and G. Verbic, "Foundations and Challenges of Low-Inertia Systems," in *2018 Power Systems Computation Conference (PSCC)*. IEEE, June 2018, pp. 1–25.

[2] N. Hatziargyriou, J. Milanovic *et al.*, "Definition and classification of power system stability – revisited & extended," *IEEE Transactions on Power Systems*, vol. 36, no. 4, pp. 3271–3281, 2021.

[3] ENTSO-E, "The inertia challenge in europe — present and long-term perspective," Ten-Year Network Development Plan 2020, Tech. Rep., 2021.

[4] U. Markovic, O. Stanojev, P. Aristidou, E. Vrettos, D. Callaway, and G. Hug, "Understanding small-signal stability of low-inertia systems," *IEEE Transactions on Power Systems*, vol. 36, no. 5, pp. 3997–4017, 2021.

[5] A. Yazdani and R. Iravani, *Voltage-sourced converters in power systems: modeling, control, and applications*. John Wiley & Sons, 2010.

[6] J. Rocabert, A. Luna, F. Blaabjerg, and P. Rodriguez, "Control of power converters in AC microgrids," *IEEE transactions on power electronics*, vol. 27, no. 11, pp. 4734–4749, 2012.

[7] T. Ackermann, T. Prevost, V. Vittal, A. J. Roscoe, J. Matevosyan, and N. Miller, "Paving the Way: A Future Without Inertia Is Closer Than You Think," *IEEE Power and Energy Magazine*, vol. 15, no. 6, pp. 61–69, 2017.

[8] B. Barac, M. Krpan, T. Capuder, and I. Kuzle, "Modeling and Initialization of a Virtual Synchronous Machine for Power System Fundamental Frequency Simulations," *IEEE Access*, vol. 9, pp. 160 116–160 134, 2021.

[9] M. Krpan and I. Kuzle, "Introducing low-order system frequency response modelling of a future power system with high penetration of wind power plants with frequency support capabilities," *IET Renewable Power Generation*, vol. 12, no. 13, pp. 1453–1461, oct 2018.

[10] European Commission, "Commission Regulation (EU) 2017/1485 of 2 August 2017 establishing a guideline on electricity transmission system operation)," Aug. 2017, legislative Body: ENER, COM.

[11] M. Krpan and I. Kuzle, "Dynamic characteristics of virtual inertial response provision by DFIG-based wind turbines," *Electric Power Systems Research*, vol. 178, p. 106005, jan 2020.

[12] J. Ma, Y. Qiu, Y. Li, W. Zhang, Z. Song, and J. S. Thorp, "Research on the impact of DFIG virtual inertia control on power system small-signal stability considering the phase-locked loop," *IEEE Transactions on Power Systems*, vol. 32, no. 3, pp. 2094–2105, 2017.

[13] G. De Carne, M. Langwasser *et al.*, "Which Deepness Class Is Suited for Modeling Power Electronics?: A Guide for Choosing the Right Model for Grid-Integration Studies," *IEEE Industrial Electronics Magazine*, vol. 13, no. 2, pp. 41–55, jun 2019.

[14] G. De Carne, G. Lauss *et al.*, "On Modeling Depths of Power Electronic Circuits for Real-Time Simulation - A Comparative Analysis for Power Systems," *IEEE Open Access Journal of Power and Energy*, vol. 9, pp. 76–87, 2022.

[15] P. Anderson and M. Mirheydar, "A low-order system frequency response model," *IEEE Transactions on Power Systems*, vol. 5, no. 3, pp. 720–729, 1990.

[16] Z. Zhang, E. Du *et al.*, "Modeling frequency response dynamics in power system scheduling," *Electric Power Systems Research*, vol. 189, p. 106549, Dec. 2020.

[17] L. Badesa, F. Teng, and G. Strbac, "Optimal portfolio of distinct frequency response services in low-inertia systems," *IEEE Transactions on Power Systems*, vol. 35, no. 6, pp. 4459–4469, 2020.

[18] M. Paturet, U. Markovic, S. Delikaraoglou, E. Vrettos, P. Aristidou, and G. Hug, "Stochastic unit commitment in low-inertia grids," *IEEE Transactions on Power Systems*, vol. 35, no. 5, pp. 3448–3458, Sep. 2020.

[19] RG-CE System Protection & Dynamics Sub Group, "Frequency stability evaluation criteria for the synchronous zone of continental europe," ENTSO-E, Tech. Rep., 2016.

[20] T. Baškarad, I. Kuzle, and N. Holjevac, "Photovoltaic system power reserve determination using parabolic approximation of frequency response," *IEEE Transactions on Smart Grid*, vol. 12, no. 4, pp. 3175–3184, 2021.

[21] E. I. Batzelis, G. E. Kampitsis, and S. A. Papathanassiou, "Power reserves control for pv systems with real-time mpp estimation via curve fitting," *IEEE Transactions on Sustainable Energy*, vol. 8, no. 3, pp. 1269–1280, 2017.

[22] J. Hu, L. Sun, X. Yuan, S. Wang, and Y. Chi, "Modeling of Type 3 Wind Turbines With df/dt Inertia Control for System Frequency Response Study," *IEEE Transactions on Power Systems*, vol. 32, no. 4, pp. 2799–2809, jul 2017.

[23] R. Quan and W. Pan, "A Low-Order System Frequency Response Model for DFIG Distributed Wind Power Generation Systems Based on Small Signal Analysis," *Energies*, vol. 10, no. 5, p. 657, 2017.

[24] B. Wen, D. Boroyevich, P. Mattavelli, Z. Shen, and R. Burgos, "Influence of phase-locked loop on input admittance of three-phase voltage-source converters," in *2013 Twenty-Eighth Annual IEEE Applied Power Electronics Conference and Exposition (APEC)*, 2013, pp. 897–904.

[25] B. Wen, D. Boroyevich, R. Burgos, P. Mattavelli, and Z. Shen, "Analysis of d-q small-signal impedance of grid-tied inverters," *IEEE Transactions on Power Electronics*, vol. 31, no. 1, pp. 675–687, 2016.

[26] C. Zhang, X. Wang, and F. Blaabjerg, "Analysis of phase-locked loop influence on the stability of single-phase grid-connected inverter," in *2015 IEEE 6th International Symposium on Power Electronics for Distributed Generation Systems (PEDG)*, 2015, pp. 1–8.

[27] X. Wang, L. Harnefors, and F. Blaabjerg, "Unified impedance model of grid-connected voltage-source converters," *IEEE Transactions on Power Electronics*, vol. 33, no. 2, pp. 1775–1787, 2018.

[28] F. Hans, W. Schumacher, and L. Harnefors, "Small-signal modeling of three-phase synchronous reference frame phase-locked loops," *IEEE Transactions on Power Electronics*, vol. 33, no. 7, pp. 5556–5560, 2018.

[29] S. Golestan, J. M. Guerrero, and J. C. Vasquez, "Three-phase plls: A review of recent advances," *IEEE Transactions on Power Electronics*, vol. 32, no. 3, pp. 1894–1907, 2017.

[30] J. Machowski, Z. Lubosny, J. W. Bialek, and J. R. Bumby, *Power system dynamics: stability and control*, 3rd ed. John Wiley & Sons, 2020.

[31] Y. Wang, G. Delille, X. Guillaud, F. Colas, and B. François, "Real-time simulation: The missing link in the design process of advanced grid equipment," in *IEEE PES General Meeting*, 2010, pp. 1–8.

[32] F. Blaabjerg, R. Teodorescu, M. Liserre, and A. V. Timbus, "Overview of control and grid synchronization for distributed power generation systems," *IEEE Transactions on Industrial Electronics*, vol. 53, no. 5, pp. 1398–1409, oct 2006.

[33] M. Krpan and I. Kuzle, "The mathematical model of a wind power plant and a gas power plant," *Journal of Energy*, vol. 66, pp. 69–86, 2017.

[34] L. Harnefors, X. Wang, A. G. Yepes, and F. Blaabjerg, "Passivity-based stability assessment of grid-connected vscs—an overview," *IEEE Journal of Emerging and Selected Topics in Power Electronics*, vol. 4, no. 1, pp. 116–125, 2016.